Polymers

International Edition: DOI: 10.1002/anie.201603532
German Edition: DOI: 10.1002/ange.201603532

# Molecular Engineering of Conjugated Polybenzothiadiazoles for Enhanced Hydrogen Production by Photosynthesis

*Can Yang[+], Beatriz Chiyin Ma[+], Linzhu Zhang, Sen Lin, Saman Ghasimi, Katharina Landfester, Kai A. I. Zhang,* and Xinchen Wang**

**Abstract:** *The search for metal-free organic photocatalysts for $H_2$ production from water using visible light remains a key challenge. Reported herein is a molecular structural design of pure organic photocatalysts, derived from conjugated polybenzothiadiazoles, for photocatalytic $H_2$ evolution using visible light. By alternating the substitution position of the electron-withdrawing benzothiadizole unit on the phenyl unit as a comonomer, various polymers with either one- or three-dimensional structures were synthesized and the effect of the molecular structure on their catalytic activity was investigated. Photocatalytic $H_2$ evolution efficiencies up to 116 $\mu mol\,h^{-1}$ were observed by employing the linear polymer based on a phenyl-benzothiadiazole alternating main chain, with an apparent quantum yield (AQY) of 4.01 % at 420 nm using triethanolamine as the sacrificial agent.*

The development of visible-light photocatalysts for the conversion solar energy into chemical energy remains a key target of modern materials science, and is best guided by a fundamental understanding of the structural impact on functional properties.[1–3] Various photocatalytic systems have been intensely investigated in recent years. Besides metal-based photocatalysts, such as inorganic semiconductors or organometal complexes, pure organic photocatalytic systems have gained much attention recently.[4–7] Among them, binary carbon nitrides, a state-of-art example, have been wildly applied as metal-free photocatalysts because of their promising electronic and optical properties.[8–10]

Another emerging class of metal-free photocatalysts, conjugated polymers, is of particular interest because their semiconductor properties are easily tuned by modification of the band gap, band positions, and p/n character through an apprpriate choice of the donor and acceptor.[11,12] The processability of organic photocatalysts allows device fabrication of photosynthetic units. Indeed, recent research describes several design strategies for enhancing the photocatalytic activities of conjugated polymers for light-induced chemical transformations.[13–18] Some strategies include variation of chemical composition by copolymerization, band-gap alignment by microstructural modification, or nanostructuring by control of the porosity.[19,20] However, the number of examples on which conjugated polymers werer used for $H_2$ production, through photosynthesis, from either water or organic feedstocks with visible light, is very small.[21–23] Polypenylenes and poly(azomethines) were reported for $H_2$ evolution, but they are most active in UV light and demonstrate moderate activity.[21,23] Recently, the group of Cooper developed a series of promising pyrene-based copolymers as photocatalysts for $H_2$ evolution, having tunable optical gaps of 1.94–2.95 eV, and the best $H_2$ evolution rate of 17.4 $\mu mol\,h^{-1}$.[22] Considering the wide number of conjugated polymers and the variety of structural variations which can be made synthetically, further development of more efficient organic photocatalysts for enhanced $H_2$ generation, by photosynthesis, is envisaged. Indeed, planarized fluorene-type polymers were very recently explored by the same group for enhanced $H_2$ evolution with visible light.[24]

Herein we report on a molecular structure design strategy of electron-donor–acceptor conjugated polymers for visible-light-promoted $H_2$ evolution. Starting from a simple phenyl unit, benzothiadiazole, an electron-withdrawing unit, was incorporated into the polymer backbone at different positions on the phenyl ring, thus leading to polymers varying from one-dimensional (1D) linear polymers to three-dimensional (3D) networks. A study on the effect of the molecular structure of the conjugated polybenzothiadiazole on their ability to function as organic photocatalysts for $H_2$ evolution with visible light was conducted. It was observed that the linear polymer based on an alternating phenyl-benzothiadiazole main chain demonstrated an enhanced photocatalytic efficiency with a hydrogen evolution rate (HER) of 116 $\mu mol\,h^{-1}$, as well as high stability and reusability.

In Scheme 1, the structures of the polymer series are displayed. Two series of conjugated polybenzothiadiazoles were synthesized by Suzuki–Miyaura cross-coupling polycondensation reactions using 4,7-dibromobenzo[*c*]-[1,2,5]thiadiazole (BT) with either benzene-1,4-diboronic or 1,3,5-phenyltriboronic acid tris(pinacol) ester as a comonomer. In particular, the 1D linear polymer B-BT-1,4 served as a starting material, and the BT units were coupled at the 1,4-positions on the phenyl ring in the polymer main chain. The polymers in series 1 were obtained by variation of the substitution position on the phenyl ring, thus resulting in the 3D polymer networks B-BT-1,2,4, B-BT-1,3,5, and B-BT-1,2,4,5. To precisely investigate the influence of the 3D

[*] C. Yang,[+] L. Zhang, Dr. S. Lin, Prof. X. Wang
State Key Laboratory of Photocatalysis on Energy and Environment
College of Chemistry, Fuzhou University
Fuzhou 350002 (P.R. China)
E-mail: xcwang@fzu.edu.cn
B. C. Ma,[+] S. Ghasimi, Prof. K. Landfester, Dr. K. A. I. Zhang
Max Planck Institute for Polymer Research
Ackermannweg 10, 55128 Mainz (Germany)
E-mail: kai.zhang@mpip-mainz.mpg.de
[+] These authors contributed equally to this work.

Supporting information for this article can be found under: http://dx.doi.org/10.1002/anie.201603532.

  

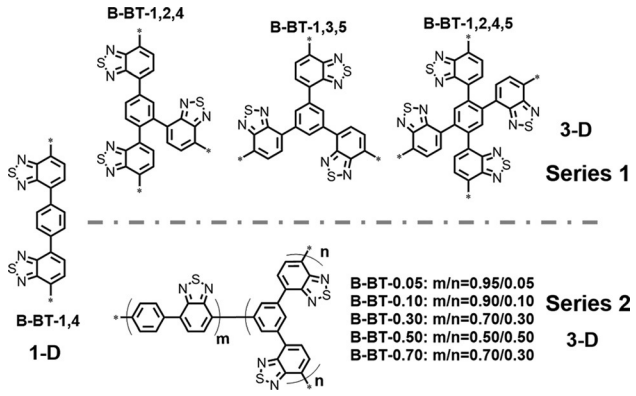


***Scheme 1.*** Structures of two series of polybenzothiadiazoles with different molecular designs.

network skeleton during the photocatalytic process of $H_2$ evolution, another series of polybenzothiadiazoles were synthesized by gradually increasing the number of 1,3,5-functionalized phenyl units, used as a comonomer, in the backbone of B-BT-1,4, thus resulting in the polymer series 2. The detailed procedures and characterization data are described in the Supporting Information.

The polymers of both series were obtained as dark yellow powders which were insoluble in all common organic and aqueous solvents tested. The polymers in series 1 showed a variation of morphologies with a fused particle-like shape for B-BT-1,2,4 and B-BT-1,2,4,5 and fused fiber shape for B-BT-1,3,5, while the linear polymer B-BT-1,4 showed a non-specific fused flake-like shape (see Figures S1 and S2 in the Supporting Information). The polymers in series 2 showed a morphology similar to that of B-BT-1,4 except for B-BT-0.70 which had a fused particle-like shape. Solid-state $^{13}C$/MAS NMR spectra showed similar signals at $\delta = 153$ ppm, which can be assigned to the carbon atom adjacent the nitrogen atom of the BT units for all polymers (see Figures S3–S11). The signals between $\delta = 115$ and 146 ppm can be assigned to the aromatic carbon atoms in the BT unit. Notably, for the polymers in series 2, the chemical shift at $\delta = 137$ ppm, which can be assigned to the aromatic carbon atoms of the phenyl comonomer, were gradually fused with the other carbon signals by introducing more 1,3,5-functionalized phenyl units as crosslinks to the polymer backbone. This result shows the extension of the crosslinked structure throughout the *meta*-position of the phenyl units in the polymer backbone structure.

Transmission electron microscopy (TEM) and the fast Fourier transformation (FFT) measurements of the polymers showed no sign of crystallinity (see Figure S12), and the powder X-ray diffraction (PXRD) profile reveals an amorphous character (see Figure S13). Interestingly, the nitrogen gas absorption measurements revealed that the linear polymer B-BT-1,4 was slightly porous (Table 1; see Figure S14) with a Brunauer–Emmett–Teller (BET) surface area of about 39 $m^2 g^{-1}$ and a pore diameter of 4.0 nm in the mesopore range caused by a molecular twist combined with a π–π stacking effect, thus leading to a certain pore formation in the solid polymer. By comparison, B-BT-1,2,4, B-BT-1,3,5, and B-BT-1,2,4,5 in series 1 showed microporous properties with BET surface areas ranging from 40 to 280 $m^2 g^{-1}$ and a similar pore diameter of about 1.5 nm. The polymers in series 2 did not show a clear trend of porosity by gradually increasing the number of the crosslink unit in the polymer backbone. The BET surface areas ranged from 40 to 129 $m^2 g^{-1}$ with pore sizes ranging from about 3.8 to 10.7 nm.

***Table 1:*** Porosity data and electrochemical properties of the polymers.

| Polymer | $S_{BET}$[a] [$m^2 g^{-1}$] | PD[b] [nm] | PV[c] [$m^3 g^{-1}$] | HOMO[d]/ LUMO[e] [V vs. NHE] | OG[f] [eV] | HER[g] [μmol $h^{-1}$] |
|---|---|---|---|---|---|---|
| B-BT-1,4 | 39 | 0.14 | 4.0 | 1.28/−0.89 | 2.17 | 116 |
| B-BT-1,2,4 | 17 | 0.03 | 4.5 | 1.27/−0.98 | 2.25 | 1.3 |
| B-BT-1,3,5 | 280 | 0.37 | 1.5 | 1.41/−1.03 | 2.44 | 20 |
| B-BT-1,2,4,5 | 40 | 0.06 | 1.5 | 1.23/−1.09 | 2.32 | 0.4 |
| B-BT-0.05 | 58 | 0.10 | 3.8 | 1.25/−0.95 | 2.20 | 82 |
| B-BT-0.10 | 93 | 0.24 | 3.8 | 1.24/−0.97 | 2.21 | 50 |
| B-BT-0.30 | 129 | 0.51 | 4.5 | 1.23/−0.99 | 2.22 | 39 |
| B-BT-0.50 | 40 | 0.20 | 10.7 | 1.23/−1.00 | 2.23 | 19 |
| B-BT-0.70 | 84 | 0.20 | 3.8 | 1.27/−1.02 | 2.29 | 19 |

[a] Specific surface area calculated from the $N_2$ adsorption isotherm. [b] Pore diameter. [c] Pore volume. [d] Derived by extracting the LUMO level from the optical gap. [e] Determined by cyclic voltammetry (the standard error of LUMO position is ±0.008 eV from three measurements). [f] Optical gap (OG) derived from the absorption edges. [g] Reaction conditions: 50 mg polymer, 110 mL TEOA/$H_2O$ (10/100), 3 wt% Pt, 300 W Xe lamp with cut-off filter >420 nm.

The FTIR spectra showed typical signals at 1440 and 1490 $cm^{-1}$, which can be assigned to the skeleton vibration of the aromatic rings in the polymers. The signals at 1340 and 1570 $cm^{-1}$ can be assigned to the C=N and N−S stretching modes, respectively, of the BT unit (see Figures S16 and S17). Thermogravimetric analysis of the polymers revealed different thermal stabilities of the polymers with an overall tendency of higher stability for the linear polymer B-BT-1,4 and its 3D counterparts in series 2 (see Figure S18).

The UV/vis diffuse reflectance spectra (DRS) of the polymers are displayed in Figures 1 a,b. Both series showed broad absorption range in the visible region. B-BT-1,4 exhibited the largest adsorption area across both polymer series, whereas its 3D counterpart, B-BT-1,3,5, showed the narrowest absorption range. A clear tendency for optical absorption of the 3D structure could be observed for series 2. By increasing the amount of the crosslinker in the polymer backbone, that is, by expanding the 3D character of the polymer, the absorption ranges of the polymers decreased gradually (Figure 2 b). Optical gaps between about 2.1 and 2.5 eV could be derived from the absorption edges. The linear polymer B-BT-1,4 exhibited the narrowest band gap of 2.17 eV. In comparison, the 3D polymer networks in both series showed broader band gaps, with B-BT-1,3,5 possessing the broadest optical gap of 2.42 eV. The optical and electrochemical properties for both polymer series are also listed in Table 1.

To further study the energy band structures of the polymers, cyclic voltammetry (CV) measurements were conducted, and revealed different energy levels within the

  

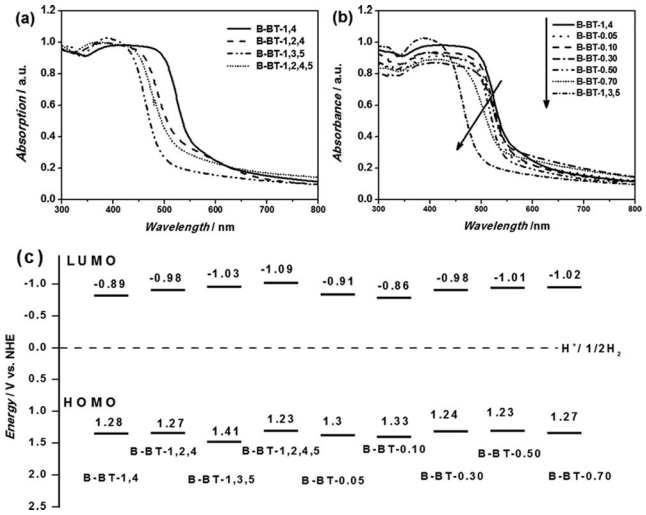


***Figure 1.*** UV/Vis diffuse reflectance spectra (DRS) of polymers in series 1 (a) and series 2 (b). c) HOMO and LUMO band position of the polymers (the standard error of LUMO position is $\pm 0.008$ eV from three measurements).

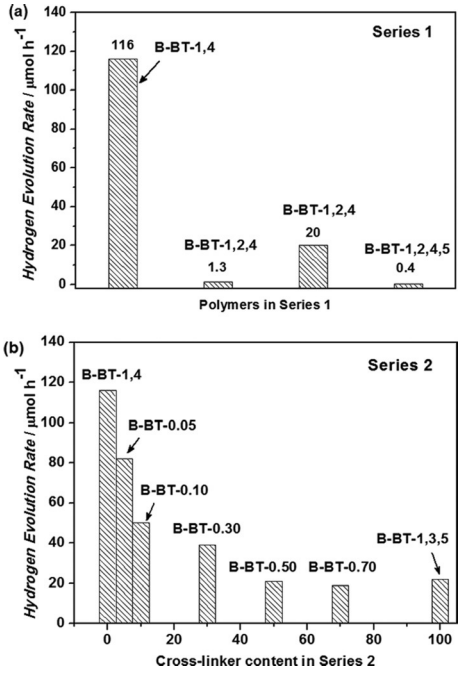


***Figure 2.*** $H_2$ evolution rates using polymers in Series 1 (a) and Series 2 (b).

polymer series (see Figures S19 and S20). The overall tendency was that the 3D polymers in series 1 exhibited higher LUMO levels than that of the linear polymer B-BT-1,4 ($-0.89$ V vs. NHE; Figure 1c; Table 1). The lower-energy band of B-BT-1,4 is likely caused by the better extended conjugated system of the linear chain relative to that of its 3D counterpart, which has a rather twisted structure and thus a narrower band gap. This feature was supported by theoretical calculations of five possible 1D and 3D structures (see Figures S29 and S30). Results reveal that donor–acceptor characteristics are more obvious in the charge density of the 1D B-BT-1,4 structure than those in the 3D B-BT-1,3,5 twisted structures, which can in principle decrease the π-conjugated system and reduce charge mobility. This data provides additional proof to explain the improved performance of B-BT-1,4 over B-BT-1,3,5.

We further examined the photo-electrochemical properties of the polymers by photocurrent measurement (see Figure S21). The linear B-BT-1,4 exhibited an enhanced photocurrent by a factor of four when compared to its 3D counterpart B-BT-1,3,5, thus indicating an improved light-induced electronic conductivity, as well as charge transfer and charge separation in the linear polymer backbone structure B-BT-1,4 compared to the 3D structural variation.

The photocatalytic activity of the polybenzothiadiazoles in $H_2$ evolution from water in the presence of the sacrificial electron donor (triethanolamine; TEOA) was then determined. The HER of B-BT-1,4 was about 12 μmol $h^{-1}$ under visible-light irradiation ($\lambda > 420$ nm, for experimental details see the Supporting Information). Under the optimized reaction conditions, employing about 3 wt% Pt as the cocatalyst, a tenfold higher HER of 116 μmol $h^{-1}$ was achieved (Figure 2a). A direct comparison between B-BT-1,4 and fluorene-type polymers,[24] which have a high photoactivity, was performed under the same reaction conditions in our experimental set-up. Pt/B-BT-1,4 has a AQY of 4.01% at 420 nm for $H_2$ evolution when using triethanolamine as the sacrificial agent, whereas it is 2.62 and 2.48% for P7 (dibenzo[*b*,*d*]thiophene sulfone co-polymer) and Pt/P7, respectively (see Table S3; the P7 sample was kindly supplied by the authors of Ref. [24]). When using a triethylamine/methanol mixture as the sacrificial agents, P7 had the highest AQY of 6.61% (it is 5.38% for Pt/B-BT-1,4; Table S4). Clearly, the AQY depends on the type of sacrificial agent, and it is a remarkable observation that P7 and CP-CMP-10[22] can photocatalyze $H_2$ evolution without the Pt cocatalyst. A negative microstructural effect on the catalytic activity of the polymers was observed when employing the 3D polymers of series 1 as catalysts. In particular, the 3D polymer networks B-BT-1,2,4 and B-BT-1,2,4,5 only showed minimal HERs of 1.3 and 0.4 μmol $h^{-1}$, respectively, while B-BT-1,3,5 showed a moderate HER of 20 μmol $h^{-1}$.

To precisely study the 3D structural influence on the catalytic efficiency in $H_2$ production, the polymers in series 2 were investigated. It could be clearly observed that by gradually introducing the crosslinker into the polymer backbone based on B-BT-1,4, the HERs of the polymers decreased, thus indicating that the 3D character here could not effectively enhance the photocatalytic activity of the polymer series. This behavior could be explained by the fact that the LUMO levels, that is, the reduction potentials for all polymers, were sufficient enough for reducing $H^+$ to 1/2 $H_2$ with over-potentials between and 0.9 and 1 eV. These levels did not make a significant difference in their catalytic efficiencies. The main active factor should be the light-induced electron mobility and electron transfer within the polymers, and the linear polymer B-BT-1,4 demonstrated its superior properties compared to the other polymers in both series. Another additional factor could be the absorption

  

range of B-BT-1,4 in the visible region, which was broader than that for the other polymers.

Figure 3a shows the wavelength dependence of the AQY of B-BT-1,4 for $H_2$ production, thus indicating the correspondence of its photocatalytic activity in $H_2$ evolution with its maximal absorption at different wavelengths. Repeat experiments were conducted to demonstrate the stability and reusability of the polymers as photocatalysts. B-BT-1,4 could be reused for five additional cycles for 30 h without loss in its catalytic efficiency, by using a constant amount of the sacrificial agent (Figure 3b). No apparent change of the FT-IR spectrum of B-BT-1,4 could be observed (see Figure S22).

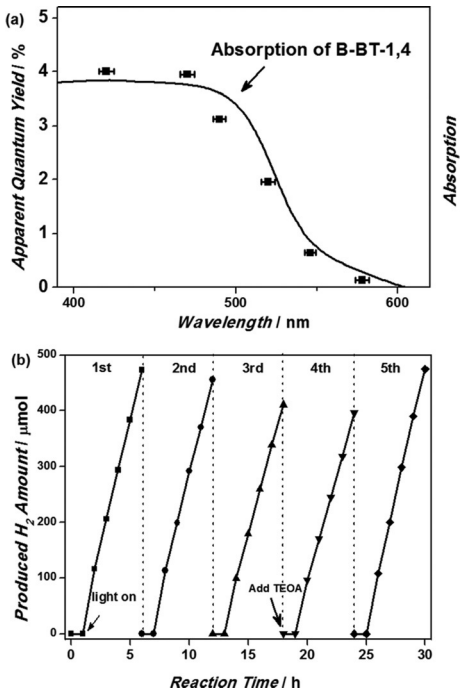


***Figure 3.*** a) Wavelength dependence of AQY on $H_2$ evolution using B-BT-1,4. b) Stability and reusability test using B-BT-1,4 as a photocatalyst under visible-light irradiation ($\lambda > 420$ nm) for 30 h.

An additional study on the effect of metal cocatalysts confirmed the superior effect of Pt nanoparticles compared to those of Pd and Rh (see Figure S23). TEM analysis of the used samples after the photocatalytic reaction revealed the formation of uniform Pt, Pd, and Rh nanoparticles on B-BT-1,4 (see Figure S25–S28)

In summary, we have presented a molecular structural design principle of conjugated polybenzodiazoles as organic, heterogeneous photocatalytic systems for visible-light-promoted $H_2$ evolution. By simply copolymerizing the electron-withdrawing benzothiadiazole units at different positions on phenyl rings, various polymers with defined energy-band structures and charge-transfer and charge-separation abilities could be obtained. Linear conjugated polymers based on a phenyl-benzothidiazole alternating main chain exhibited superior photocatalytic activity, compared to its 3D polymer network counterparts, in $H_2$ evolution from water with a HER of 116 $\mu mol\,h^{-1}$ . A negative effect on the $H_2$ evolution could be observed by introducing a 3D network character into the polymer backbone. The superior catalytic efficiency of the linear polybenzothiadiazole is likely attributed to the high efficiency of its light-induced charge-transfer, charge-separation, and electron-transfer ability. This design strategy could offer a promising platform of conjugated polymers as efficient and stable photocatalysts for $H_2$ evolution. There is a high potential for further optimization and molecular design possibilities, and it even allows the design of catalytic systems by coupling then with the oxidative photosynthetic units for water splitting and $CO_2$ fixation.

## Acknowledgments

This work was financially supported by the National Basic Research Program of China (2013CB632405) and the National Natural Science Foundation of China (21425309). B.C.M. acknowledges the financial support from DAAD, CAPES, and CNPq. K.A.I.Z. acknowledges the Max Planck Society for financial support. We thank the group of Prof. A. I. Cooper of the University of Liverpool for supplying the P7 sample for the comparison experiments.

**Keywords:** conjugation · hydrogen evolution · photocatalysis · polymers · semiconductors

**How to cite:** *Angew. Chem. Int. Ed.* **2016**, *55*, 9202–9206
*Angew. Chem.* **2016**, *128*, 9348–9352

[1] N. S. Lewis, D. G. Nocera, *Proc. Natl. Acad. Sci. USA* **2006**, *103*, 15729–15735.
[2] K. Maeda, K. Domen, *J. Phys. Chem. Lett.* **2010**, *1*, 2655–2661.
[3] F. E. Osterloh, *Chem. Soc. Rev.* **2013**, *42*, 2294–2320.
[4] I. Tsuji, H. Kato, H. Kobayashi, A. Kudo, *J. Am. Chem. Soc.* **2004**, *126*, 13406–13413.
[5] K. Maeda, T. Takata, M. Hara, N. Saito, Y. Inoue, H. Kobayashi, K. Domen, *J. Am. Chem. Soc.* **2005**, *127*, 8286–8287.
[6] K. Maeda, K. Teramura, D. Lu, T. Takata, N. Saito, Y. Inoue, K. Domen, *Nature* **2006**, *440*, 295–295.
[7] Q. Wang, T. Hisatomi, Q. Jia, H. Tokudome, M. Zhong, C. Wang, Z. Pan, T. Takata, M. Nakabayashi, N. Shibata, Y. Li, I. D. Sharp, A. Kudo, T. Yamada, K. Domen, *Nat. Mater.* **2016**, *15*, 611–615.
[8] X. Wang, K. Maeda, A. Thomas, K. Takanabe, G. Xin, J. M. Carlsson, K. Domen, M. Antonietti, *Nat. Mater.* **2009**, *8*, 76–80.
[9] Y. Zheng, L. Lin, B. Wang, X. Wang, *Angew. Chem. Int. Ed.* **2015**, *54*, 12868–12884; *Angew. Chem.* **2015**, *127*, 13060–13077.
[10] D. J. Martin, P. J. T. Reardon, S. J. A. Moniz, J. Tang, *J. Am. Chem. Soc.* **2014**, *136*, 12568–12571.
[11] A. G. Slater, A. I. Cooper, *Science* **2015**, *348*, aaa8075.
[12] H. Xu, J. Gao, D. Jiang, *Nat. Chem.* **2015**, *7*, 905–912.
[13] C. Gu, N. Huang, Y. Chen, H. Zhang, S. Zhang, F. Li, Y. Ma, D. Jiang, *Angew. Chem. Int. Ed.* **2016**, *55*, 3049–3053; *Angew. Chem.* **2016**, *128*, 3101–3105.
[14] S. Dalapati, M. Addicoat, S. Jin, T. Sakurai, J. Gao, H. Xu, S. Irle, S. Seki, D. Jiang, *Nat. Commun.* **2015**, *6*, 7786.
[15] M. Shalom, S. Inal, C. Fettkenhauer, D. Neher, M. Antonietti, *J. Am. Chem. Soc.* **2013**, *135*, 7118–7121.
[16] T. Simon, N. Bouchonville, M. J. Berr, A. Vaneski, A. Adrović, D. Volbers, R. Wyrwich, M. Döblinger, A. S. Susha, A. L. Rogach, F. Jäckel, J. K. Stolarczyk, J. Feldmann, *Nat. Mater.* **2014**, *13*, 1013–1018.

  

[17] Z. J. Wang, S. Ghasimi, K. Landfester, K. A. I. Zhang, *Adv. Mater.* **2015**, *27*, 6265 – 6270.
[18] K. Zhang, D. Kopetzki, P. H. Seeberger, M. Antonietti, F. Vilela, *Angew. Chem. Int. Ed.* **2013**, *52*, 1432 – 1436; *Angew. Chem.* **2013**, *125*, 1472 – 1476.
[19] C. Pei, T. Ben, Y. Li, S. Qiu, *Chem. Commun.* **2014**, *50*, 6134 – 6136.
[20] J. X. Jiang, A. Trewin, D. J. Adams, A. I. Cooper, *Chem. Sci.* **2011**, *2*, 1777 – 1781.
[21] M. G. Schwab, M. Hamburger, X. L. Feng, J. Shu, H. W. Spiess, X. C. Wang, M. Antonietti, K. Mullen, *Chem. Commun.* **2010**, *46*, 8932 – 8934.
[22] R. S. Sprick, J.-X. Jiang, B. Bonillo, S. Ren, T. Ratvijitvech, P. Guiglion, M. A. Zwijnenburg, D. J. Adams, A. I. Cooper, *J. Am. Chem. Soc.* **2015**, *137*, 3265 – 3270.
[23] L. Stegbauer, K. Schwinghammer, B. V. Lotsch, *Chem. Sci.* **2014**, *5*, 2789 – 2793.
[24] R. S. Sprick, B. Bonillo, R. Clowes, P. Guiglion, N. J. Brownbill, B. J. Slater, F. Blanc, M. A. Zwijnenburg, D. J. Adams, A. I. Cooper, *Angew. Chem. Int. Ed.* **2016**, *55*, 1792 – 1796; *Angew. Chem.* **2016**, *128*, 1824 – 1828.

Received: April 12, 2016
Revised: May 12, 2016
Published online: June 15, 2016

  